K. Mols, I. Verpoest,* and E. Aernoudt**

Multiaxial Fatigue of Anisotropic Carbon Steel Wire

REFERENCE Mols, K., Verpoest, I., and Aernoudt, E., **Multiaxial fatigue of anisotropic carbon steel wire**, *Biaxial and Multiaxial Fatigue*, EGF 3 (Edited by M. W. Brown and K. J. Miller), 1989, Mechanical Engineering Publications, London, pp. 231–244.

ABSTRACT The paper first describes a computer controlled multiaxial fatigue test facility, designed for automatic crack growth and threshold measurements. The equipment is used for the study of the crack growth behaviour of multiaxially loaded steel wire having various grades of anisotropy. This mechanical anisotropy, caused by the wire drawing operation, is investigated in terms of 'microstructural' and 'crystallographic' texture and is correlated with the crack growth data.

Introduction

As has been reported during a previous multiaxial fatigue conference (**1**), fatigue crack growth of multiaxially loaded steel wire shows an anomalous behaviour that can only be understood when the anisotropy of the material is taken into account. It was found that, during constant amplitude fatigue tests of isotropic steel wires (in an annealed condition) a maximum tensile stress criterion dictates the crack growth direction for any combination of torque and push–pull loading. However, when drawn wires are tested, crack propagation turns to a plane parallel to the wire axis, whenever a critical ratio of shear stress to tensile stress is reached. This phenomenon was observed for low carbon as well as for pearlitic steel wires.

The results of that program were, however, qualitative and only indicated that anisotropy might play a major role in crack growth behaviour. In this paper it is our aim to quantify the influence of anisotropy on crack growth. Because of the experimental difficulties, encountered when performing multiaxial fatigue tests, it was decided to automate the fatigue equipment prior to any testing.

Notation

a	Crack depth
S	Cracked area
c	Chordal length of cracked area
U	Potential drop
σ	Remote normal stress
τ	Remote shear stress

* Department of Metallurgy and Materials Engineering, Katholieke Universiteit Leuven, De Croylaan 2, 3030 Heverlee, Leuven, Belgium.

$\varkappa$ Shear to normal stress ratio
ΔK Stress intensity factor range
R Minimum to maximum load ratio
SF Multiplication factor for determination of critical crack depths during one step of load shedding
θ Angle between the normal to the crack plane and the wire axis
r_p Plastic zone size

The multiaxial test system

The experimental work was carried out on a Schenck servohydraulic test facility which enabled combined tension–torsion and internal pressure loading. At the time that this project started the machinery was equipped with a manual control and therefore the first objective was to automate the existing fatigue facility in the most efficient way: both, servo-control and data acquisition were placed under computer control which offered a wide range of testing possibilities that could only with great difficulty be achieved with simple manual control and analogue data-recording.

Figure 1 is a schematic diagram that illustrates the principle of operation of the feedback control system for a single 'loading' circuit (axial, torque, or internal pressure). The hydraulic power is delivered by the accumulator (AC) working at 280 bar. The oil flow into the double-acting actuator (or single-acting only for the internal pressure), is controlled by the servo-valve (SV), which is energised by a servo-amplifier (SA). A control variable (force, displacement, or strain (F, D, S)) is measured, conditioned by the input amplifier (IA), and fed back to the servo-controller (SA), which compares the measured quantity with the implied value given by the command signal generator (CG). This command signal generator is, in fact, a device that provides the possibility to 'construct' an output signal (O) as the sum of a static and a dynamic component: the static signal (DC) is provided by a d.c.-voltage source; the dynamic

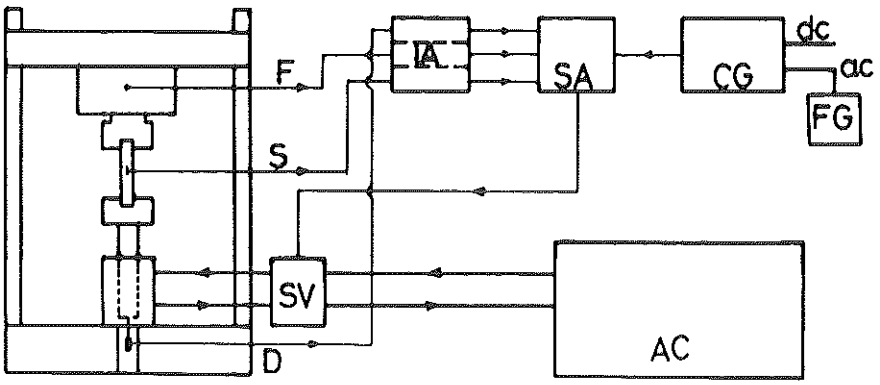

Fig 1 A servohydraulic feedback control system

component (AC) is made of a reference signal (given by a function generator, FG) which is then attenuated to the proper value.

The most straightforward method of automating the machine was to bring the function generator under computer control and to add a data acquisition system. In our opinion, a home made solution had major advantages when compared with the dedicated commercial system available at that time. It could be made more versatile, it would be accessible for later additional programming, and should fit directly to our needs.

The system we developed is based on an instrument (called Data-Harvester) that was originally designed by colleagues at the Department of Mechanical Engineering to serve in a modal analysis test stand. It is a remote controlled, modular device with fast data acquisition possibilities (on parallel input channels) and with a programmable function generator. More functional details can be found in Table 1. The Data-Harvester is controlled by a powerful microcomputer (HP series 200/300) through a 16 bit parallel interface (GPIO-bus). A driver library was written, giving users easy, high level access from Pascal programs to all the features of the device.

Several applications based on the combination of the Data-Harvester and the HP-microcomputer have been made. They range from test control and data acquisition of high speed hot torsion tests to simple data-logging programs.

The major application, however, is the fatigue software package. The core of this Pascal program is responsible for the feedback control and the operator interface and implements a 'toolkit' with auxiliary procedures that can be used (imported) in the USER module. This USER module is responsible for data acquisition and storage and can implement an algorithm or database to determine the test sequence (block loading, constant K-tests, threshold testing, etc.). The USER module is the only 'test-dependent' part of the program and can be developed separately from the core. Only at execution level have the two parts to be linked.

Table 1 General characteristics of the Data-Harvester

Output module (function generator)		
freq. 0.001 to 9999 Hz (4 digit accuracy)		
4 channels		
reference:	d.c., a.c. −10 . . . +10 volt	
1, 2, 3:	d.c. −10 . . . +10	a.c. −ref . . . +ref
	phase −180 +180	
accuracy:	12 bit d/a conversion:	1/4096 of full range
programmable waveform:	1024 points buffer	
Input modules: (A/D convertors with data buffering)		
maximum 64 inputcards connected		
sample rate:	up to 100 kHz	
accuracy:	12 bit	
gain:	1 . . . 800 times	
internal buffer:	4096 words per channel	
features as autogain, triggered input, etc.		

The Data-Harvester and the computer replace the ordinary function generator in the test facility: for each loading axis (tension, torsion, internal pressure) one input channel is used to feed back the measured signal, while the other input channels are free for additional measurements (e.g., potential drop, temperature, strain, etc.).

The software control of the command signal performed by the program core is necessary because, during a fatigue test, the response to the applied signal may alter due to structural changes in the specimen (stiffness degradation in a composite, crack growth, softening, etc.). Moreover, the response may also alter when the load level is changed. Because of these possible changes in response, a feedback algorithm is used to correct these amplitude differences. The software will not control the shape of the signal (it is much too slow for that), but it will control amplitude and mean level and, in addition, the phase correspondence in multiaxial tests.

Depending on the test frequency, this feedback algorithm is executed every second cycle (lower than 3 Hz) rising to every 10 cycles (at 50–60 Hz).

The crack growth measurement system

Probably the most successful technique for on-line crack propagation measurement is the potential drop method (2). The crack can easily be monitored with great accuracy and the measured quantity (a slowly varying electrical signal) is well suited for digitizing and, as such, for automation.

In the particular case of cracks in a cylindrical test specimen the resolution could be improved by using the a.c.-potential drop technique at higher frequencies. Because of the skin effect, the measurement will be more sensitive to variations of the impedance due to changes in the material near the surface. Furthermore, a differential measurement of a cracked versus an uncracked zone improves the signal quality and resolution. Since it is almost impossible to calculate in advance the quantitative relation between the crack propagation (increase of crack depth, increase of cracked surface) and the potential drop for the rather complex situation of cracks growing in cylindrical specimens, the relation was determined empirically. A best fit solution to a parametric expression was used

$$a = A * U^B \tag{1}$$

In this expression, a is the crack depth and U is the total potential drop caused by that crack. The parameters A and B can be calculated with a least squares algorithm. One should, however, take into account that, under combined loading conditions, the crack will not grow in a plane perpendicular to the electrical current direction (see Fig. 2), and this might influence the relation between a and U. A much better correlation was found using a parametric relation between the cracked area (S), the inclination angle (θ) and the potential drop (U)

$$S = \{1/\cos^2(\theta)\} \cdot (A + B \cdot U) \tag{2}$$

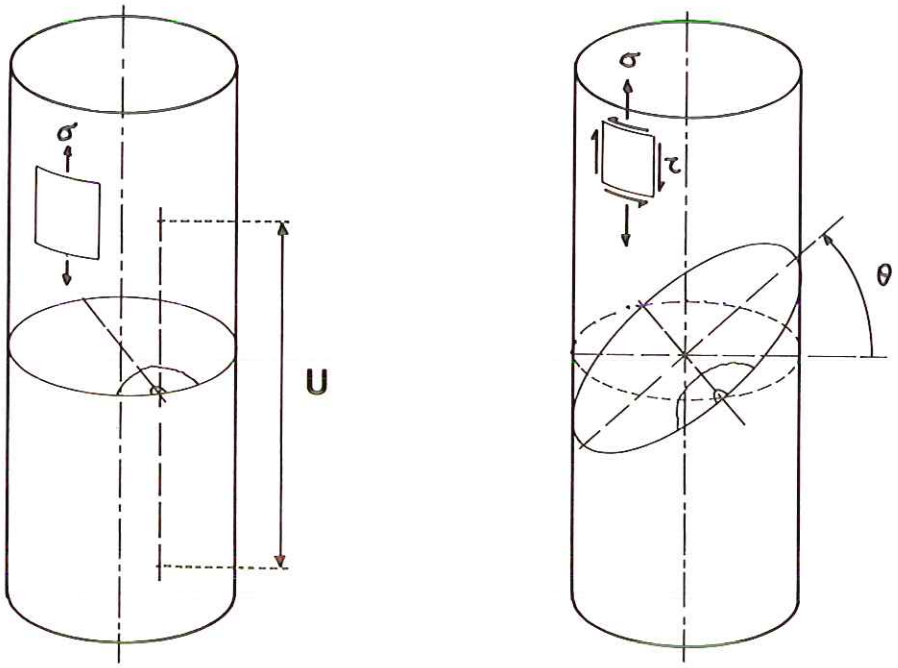

Fig 2 Orientation of cracks in multiaxial specimens

Supposing that the crack front is elliptical, the crack depth could be calculated from the cracked area when c/a and θ were known. The results, discussed later, will show that, when this parametric relation is used, no distinction can be made between data points collected during tests with different combinations of tension and torsion loading.

Figure 3 gives the calibration curves and data points using both expression (1) (Fig. 3(a)) and expression (2) (Fig. 3(b)). It is clear that the potential drop correlates much better with the cracked area than with the crack depth, since the correlation coefficient increases from 0.84 to 0.96. The cracked area can be determined from the crack depth if c/a is known. Figure 4 shows that the value of S calculated from a and c/a fits well with the experimental value. This is important since, from the inverse relation, one can calculate the crack depth from the cracked area (which is in turn determined from the potential drop).

Table 2 lists the most important features of the potential drop system used for our experiments. It should be noticed that, because of the non-linear relation between a and U, smaller crack increments can be detected at larger crack depths. This is, of course, very useful when a load shedding technique is applied for the determination of the threshold stress intensity factor.

In addition to the detection of the crack depth, the problem of implementation of a crack growth measurement module in the software package had to be solved (this is called a USER module). In our particular case the algorithm

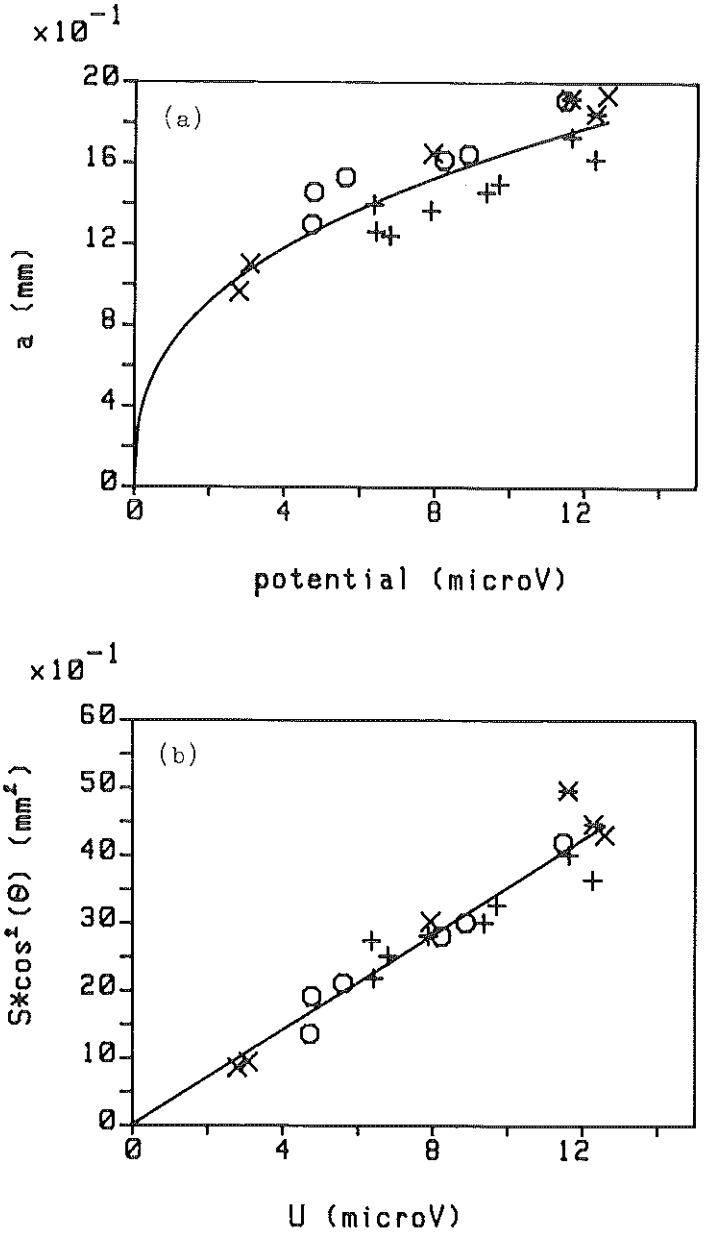

Fig 3 Potential drop calibration curves for (a) crack depth, and (b) projected crack area, under multiaxial stresses (τ/σ) of 0.0 (+), 0.5 (*), 1.0 (0), and 1.5 (x)

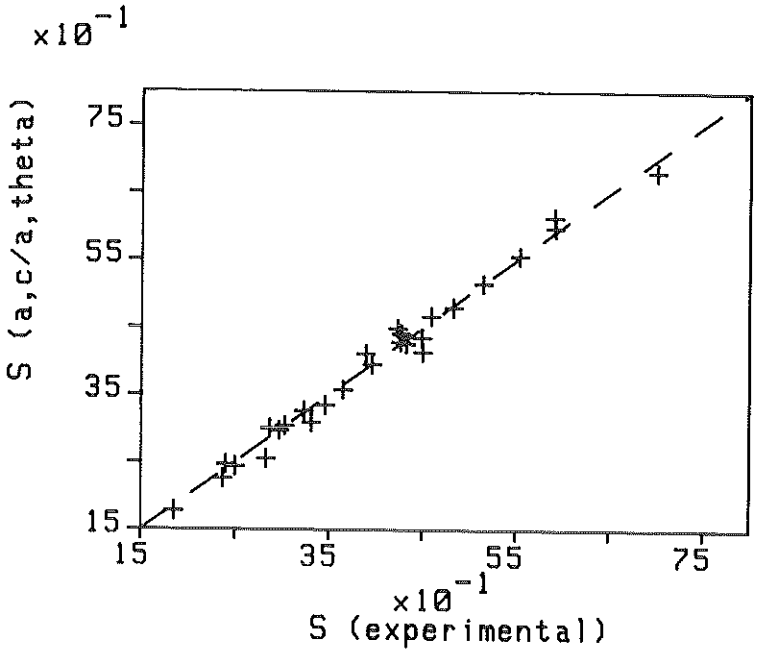

Fig 4 Correlation between experimental and calculated crack surface area

Table 2 Characteristics of the potential drop measurement

Wire diameter: 8 mm
Current source: 1 amp, 10 khz
Initial potential drop: $\approx 550\ \mu V$
Smallest detectable change: $0.05\ \mu V/5 \cdot 10^5$ cycles

	Start of test	*End of test*
$U(A-B)\ (\mu V)$	2.000	12.000
a (mm)	0.655	1.841
$U + 0.005$	2.050	12.050
$a + \delta a$	0.664	1.846
δa	0.009	0.005

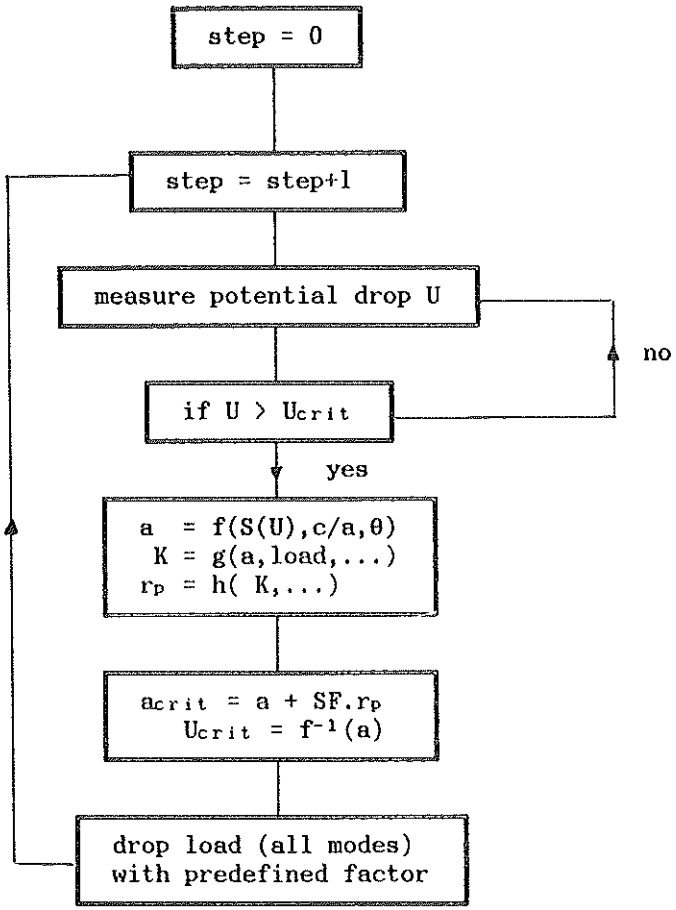

Fig 5 Load shedding algorithm

given in Fig. 5 was used. This is a typical load shedding algorithm. The crack extension is continuously monitored by measuring the related differential potential drop (U). When U reaches a critical value (U_{crit}) the load is decreased until, after a number of steps, the crack arrests. After each step the cracked area is determined from the calibration curve and the crack depth and stress intensity factor are calculated. From the latter, one can estimate the plastic zone size (r_p) ahead of the crack, which in turn is used to determine the minimal crack growth for the next load level. The safety factor used should be high enough to prevent corruption of the measurement in one step when compared to the previous step. Eventually the required crack increase is transformed into a critical potential drop. The safety factor as well as the amount by which the load is dropped can be altered during a test by the operator.

The material

In order to study the influence of anisotropy, a material was selected that could be produced in both the isotropic and anisotropic form. Furthermore, this material had to have a cylindrical shape and symmetry. Because of the loading system (push–pull and torsion), this kind of specimen should facilitate the interpretation of the measurements relating to the effect of anisotropy. A cylindrical symmetry means that a crack emanating from anywhere on the surface must give the same crack growth results, independent of the position (on the circumference) of the crack origin. Taking all those considerations into account, it was decided to use steel wire. Four different types were used, for which the most important features are given in Table 3.

In order to have the most complete understanding of the mechanical anisotropy of those materials a metallographic study, texture measurements, and monotonic mechanical tests have been performed. Some of the mechanical properties are also listed in Table 3.

The texture measurements of the patented high carbon type material and the annealed low carbon wire revealed that almost no orientation dependence of the ODF (orientation distribution function) existed; the grains have totally random crystallographic orientations. In the case of the drawn condition, a strong 'wire-type' texture was found; the crystal grains show a tendency to have their ⟨110⟩ direction parallel to the wire axis.

In addition to the crystallographic texture, grain shape and orientation of pearlite lamellae will also influence the mechanical anisotropy and the crack propagation behaviour. This has already been indicated by Verpoest (1).

The fatigue tests

Wires with a diameter of 8 mm were used. The only preparation done was straightening by stretching, and spark erosion of a semispherical notch, with a depth of less than 0.3 mm, to act as a crack initiator. Tests were always done at room temperature and in laboratory air, and with an R ratio of 0.1 in order to

Table 3 Properties of the selected test materials

Name	*LCA*	*LCD*	*HCP*	*HCD*
Condition	*Low carbon annealed*	*Low carbon drawn (78%)*	*High carbon patented*	*High carbon drawn (75%)*
% carbon	0.06	0.06	0.83	0.83
0.2% proof stress (MPa)	251	715	812	1347
tensile strength (MPa)	354	743	1309	1708
0.4% shear proof stress (MPa)	211	540	690	900
shear strength (MPa)	416	598	841	1055

prevent buckling. In the case of the multiaxial tests, the tension and torsion loading was in phase. The test frequency varied depending on the loading conditions; 40 Hz for uniaxial tests, and as low as 7 Hz for combined tests. This was due to the slender form of the specimen and the use of hydraulic clamps with a massive moment of inertia; wires have only a small resistance to torque loading which results in high rotational displacements of the hydraulic clamp at the side of the actuator. Hence, the response of the mechanical–hydraulic system becomes very poor when high frequencies (resulting in high accelerations of the clamp) are applied.

Results

The measured crack inclination was compared with the inclination of the plane of maximum principal stress (Fig. 6). It shows that, in the isotropic patented steel, cracks grow under pure Mode I as their crack plane coincides with the plane of maximum principal stress. However, for the anisotropic drawn high carbon steel, mixed mode crack growth is observed; the measured crack inclination is larger than the one calculated for pure mode I. This difference increases with increasing $\varkappa$, equal to τ/σ, where τ is the shear stress and σ the tensile stress. At the surface of the wire the mode II component becomes non-zero, while at the deepest point of the crack the mode III component becomes non-zero.

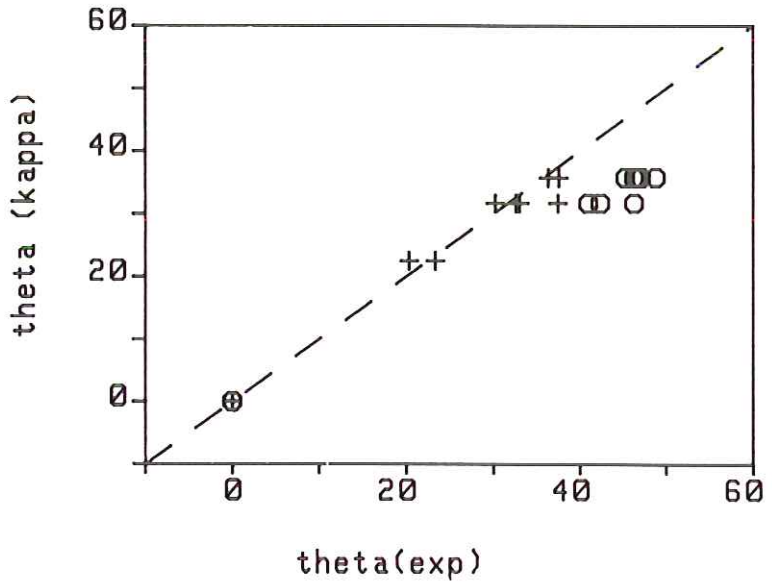

Fig 6 Correlation between measured crack inclination θ and inclination of principal stress plane $\theta(\varkappa)$, for isotropic (+) and anisotropic (0) wire

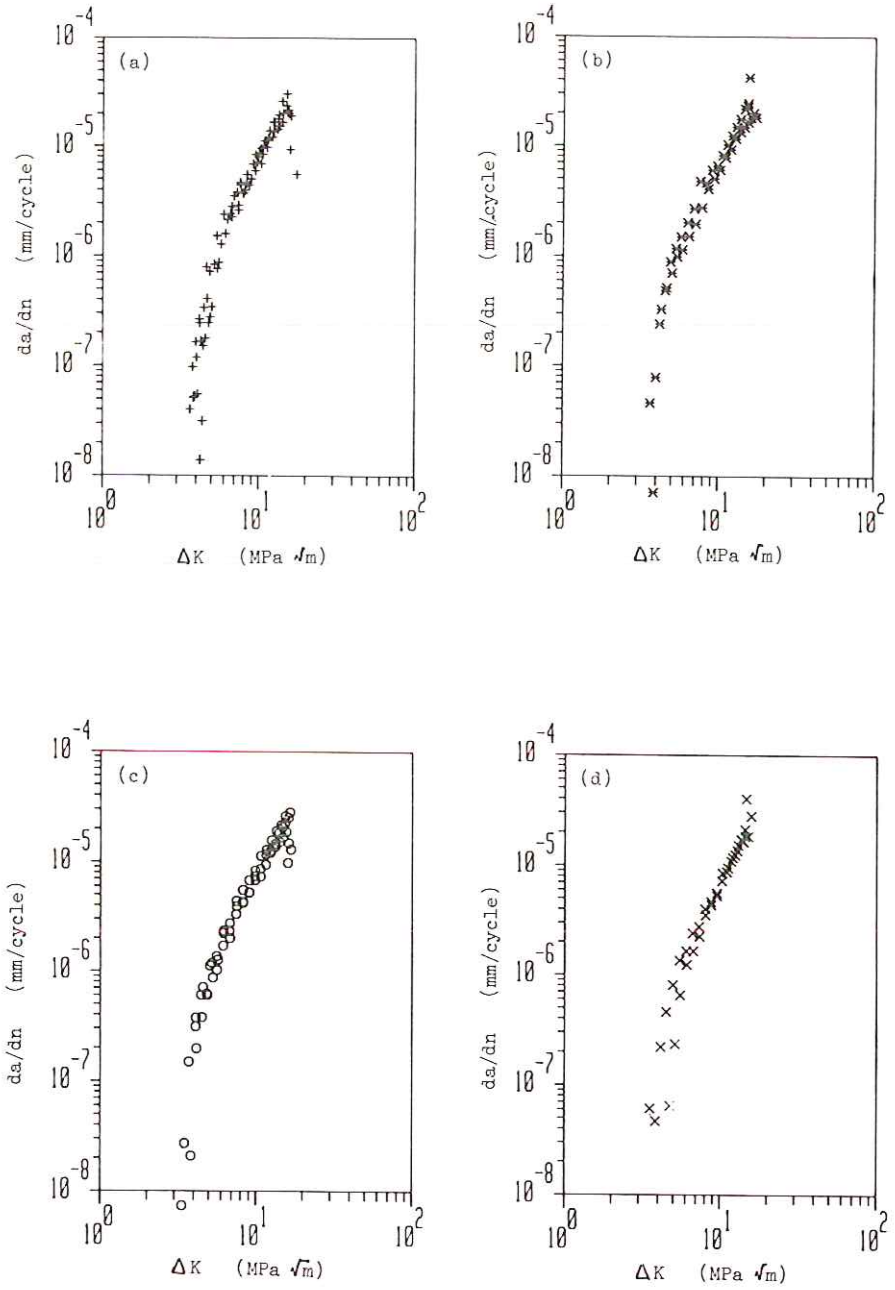

Fig 7 Dependence of crack growth rate d*a*/d*N* (mm/cycle) on stress intensity factor range ΔK_I (MPa$\sqrt{m}$) for high carbon patented steel under multiaxial stresses of: (a) $\varkappa = 0$, (b) $\varkappa = 0.5$, (c) $\varkappa = 1.0$, and (d) $\varkappa = 1.5$

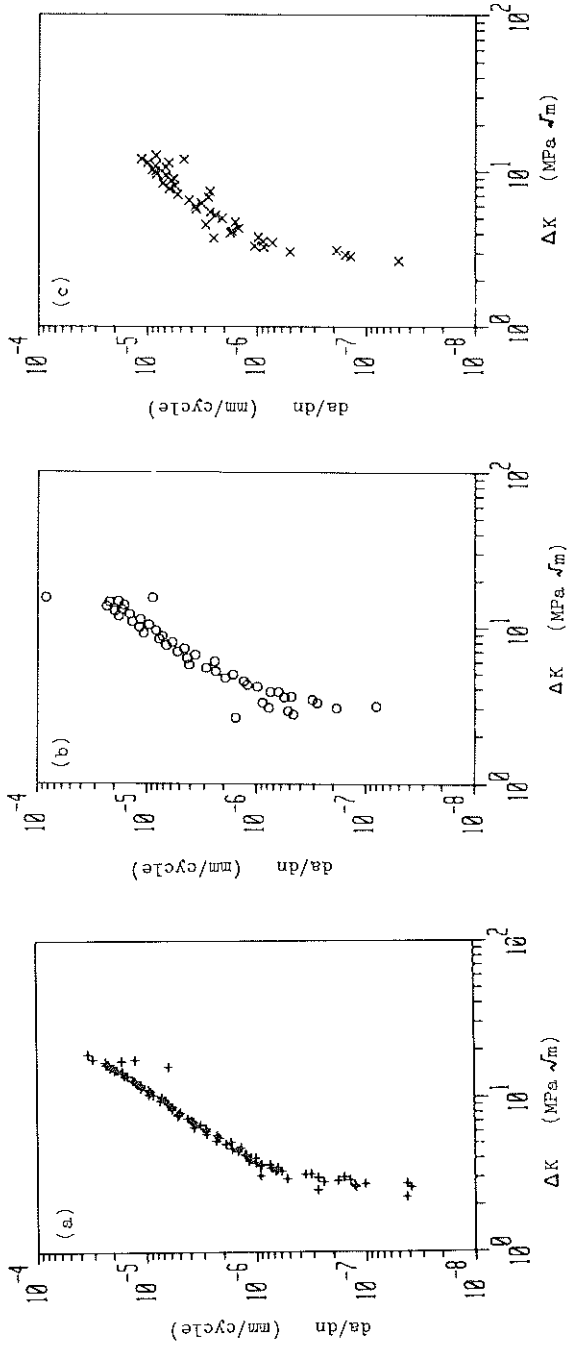

Fig 8 Dependence of crack growth rate da/dN (mm/cycle) on stress intensity factor range ΔK_I (MPa $\sqrt{m}$) for high carbon drawn wire under multiaxial stresses of (a) $\alpha = 0$, (b) $\alpha = 1.0$, and (c) $\alpha = 1.5$

Table 4 Results of the crack growth tests

Test	τ/σ	*Threshold* ($MPa\sqrt{m}$)	*Paris slope*	θ (*deg*)	c/a · *cos* (θ)
HCP	0	4.0	2.8	0	2.05
	0.5	4.0	2.8	22	2.06
	1.0	3.5	2.8	32	1.97
	1.5	4.0	2.8	37	2.03
HCD	0	2.6	2.2	0	2.09
	1.0	3.0	2.4	43	1.87
	1.5	2.6	2.2	47	1.70

Figures 7 and 8 give the crack speed, da/dn, versus the range of stress intensity factor, ΔK_I, curves for all the relevant tests, and in Table 4 the most important characteristics of these plots are summarized. An expression for the mode II stress intensity factor in this complex situation is not known, but K_I could be determined (see Appendix). This stress intensity factor was then related to the radial crack growth that is not influenced by the mode II crack displacement. Moreover, since the da/dn versus ΔK_I curves remain unchanged when altering the stress state, one can conclude that the contribution of the mode III crack growth component can be neglected.

It is also interesting to note that the shape of the crack (when projected on a plane normal to the wire axis) remains the same in the case of the patented wire, but decreases in the drawn wires. This can be seen from the $c/a \cdot \cos(\theta)$ values in Table 4.

Concluding remarks

From the experimental work now completed some major conclusions an be drawn. The crack growth in the isotropic material is always a mode I type of growth. Because of the anisotropy, mixed mode crack growth can become more favourable. In the case of the drawn wire, the crack tends to align more with the wire axis. From the crack growth curves for the anisotropic material it could be seen that irrespective of the stress state, the curves remained unchanged. This means that the radial crack growth is not influenced by the additional mode III stress component. However, the inclination of the crack (away from the plane of maximum principal stress) indicates that there is a mode II contribution to crack growth. Additional tests with other (τ/σ) ratios should provide a better understanding of these phenomena.

Appendix: The determination of the stress intensity factor range

For pure mode I loading

$$\Delta K_I = \alpha \cdot \Delta S \cdot (\pi \cdot a)^{1/2} \tag{3}$$

where

ΔS = stress range normal to the crack plane
a = crack depth
α = geometrical factor

Verpoest (3) proposed an expression for the factor α based on literature data. In that expression α was a function of the ratio of cracked area over total area of the wire $(a/2r)^2$. This idea was enlarged for cracks growing on a plane that is rotated over an angle θ from the transverse section. This leads to

$$\alpha = \alpha_1 + \alpha_2 \cdot (a/2r)^2 \cdot \cos(\theta); \quad \alpha_1 = 0.67, \quad \alpha_2 = 1.12 \tag{4}$$

The stress tensor (in crack coordinates) S^c can be derived from the stress tensor (S^w) written in a coordinate system related to the wire and a rotation matrix, $\boldsymbol{R}$

$$(S^c)_{ij} = \boldsymbol{R}_{ik} * \boldsymbol{R}_{jl} * (S^w)_{kl} \tag{5}$$

The component of S^c normal to the crack plane is then used to calculate the stress range.

References

(1) VERPOEST, I., NOTOHARDJONO, B., and AERNOUDT, E. (1985) Fatigue of steel wire under combined tensile and shear loading conditions, *Proceedings of the Multiaxial Fatigue Symposium, ASTM STP 853*, pp. 361–377.
(2) VERPOEST, I., AERNOUDT, E., DERUYTTERE, A., and NEYRINCK, M. (1981) An improved a.c. potential drop method for detecting surface microcracks during fatigue tests of unnotched specimens, *Fatigue Engng Mater. Structures*, **3**, 203–217.
(3) VERPOEST, I., AERNOUDT, E., DERUYTTERE, A., and DE BONDT, M. (1985) The fatigue threshold, surface condition and fatigue limit of steel wire, *Int. J. Fatigue*, **4**, 199–214.